

Plasma Sci. Technol. **25** (2023) 075105 (12pp) https://doi.org/10.1088/2058-6272/acbef5

A new electromagnetic probe array diagnostic for analyzing electrostatic and magnetic fluctuations in EAST plasmas

Heng LAN (兰恒)[1,2], **Tonghui SHI** (石同辉)[3], **Ning YAN** (颜宁)[3,*], **Xueqin LI** (李雪芹)[3,4], **Shi LI** (李实)[3], **Ran CHEN** (陈冉)[3], **Moyi DUAN** (段莫疑)[3,4], **Guanghai HU** (胡广海)[3], **Lunan LIU** (刘鲁南)[3], **Wei ZHANG** (张炜)[3], **Ming CHEN** (陈明)[3,4], **Yuanyang ZHENG** (郑元阳)[3], **Zhong YUAN** (袁忠)[3], **Yong WANG** (王勇)[3], **Zhanghou XU** (许张后)[3], **Liqing XU** (徐立清)[3], **Pengfei ZI** (訾鹏飞)[3], **Liang CHEN** (陈良)[3], **Shaocheng LIU** (刘少承)[3], **Donggui WU** (吴东贵)[3,4], **Genfan DING** (丁根凡)[3,4], **Lingyi MENG** (孟令义)[3], **Zhengchu WANG** (汪正初)[3], **Qing ZANG** (臧庆)[3], **Muquan WU** (吴木泉)[1,2], **Xiang ZHU** (朱翔)[1,2], **Baolong HAO** (郝保龙)[1,2], **Xiaodong LIN** (林晓东)[1], **Xiang GAO** (高翔)[1,2,3], **Liang WANG** (王亮)[3] **and Guosheng XU** (徐国盛)[3,*]

[1] College of Physics and Optoelectronic Engineering, Shenzhen University, Shenzhen 518060, People's Republic of China
[2] Advanced Energy Research Center, Shenzhen University, Shenzhen 518060, People's Republic of China
[3] Institute of Plasma Physics, Chinese Academy of Sciences, Hefei 230031, People's Republic of China
[4] Science Island Branch of Graduate School, University of Science and Technology of China, Hefei 230031, People's Republic of China

E-mail: yanning@ipp.ac.cn and gsxu@ipp.ac.cn

Received 1 October 2022, revised 14 February 2023
Accepted for publication 24 February 2023
Published 5 April 2023

Abstract

A novel electromagnetic probe array (EMPA) diagnostic, which consists of a magnetic probe array and an electrostatic probe array, has recently been developed on EAST. The EMPA is fixed near the first wall at horizontal port P. The magnetic probe array of the EMPA consists of 24 identical magnetic probes, each of them capable of measuring toroidal, poloidal and radial magnetic fluctuations simultaneously, providing additional toroidal magnetic fluctuation measurements compared with the regular magnetic probes on EAST. With a higher sampling rate and self-resonant frequency, the EMPA magnetic probes can provide higher frequency magnetic fluctuation measurements. The magnetic probe array of the EMPA is composed of two parallel layers of magnetic probes with a radial distance of 63 mm, and each layer of magnetic probes is arranged in four poloidal rows and three toroidal columns. The compact arrangement of the EMPA magnetic probe array largely improves the toroidal mode number measurement ability from $-8 \leqslant n \leqslant 8$ to $-112 \leqslant n \leqslant 112$, and also improves the high poloidal wave number measurement ability of magnetic fluctuations compared with the regular high frequency magnetic probes on EAST. The electrostatic probe array of the EMPA consists of two sets of four-tip probes and a single-tip probe array with three poloidal rows and four toroidal columns. It complements the electrostatic parameter measurements behind the main limiter and near the first wall in EAST. The engineering details of the EMPA diagnostic, including the mechanical system, the electrical system, the acquisition and control system, and the effective area calibration, are presented. The preliminary applications of the EMPA in L-mode and H-mode discharges on EAST have demonstrated that the EMPA works well for providing information on

* Authors to whom any correspondence should be addressed.

the magnetic and electrostatic fluctuations and can contribute to deeper physical analysis in future EAST experiments.

Keywords: EAST tokamak, electromagnetic probe array, magnetic fluctuations, electrostatic fluctuations

(Some figures may appear in colour only in the online journal)

1. Introduction

In fusion plasma research, magnetic probes are widely used for taking stationary and fluctuating magnetic field measurements, such as in DIII-D [1, 2], Alcator C-Mod [3], NSTX-U [4], JET [5], ASDEX Upgrade [6, 7], MAST [8], TCV [9], WEST [10], EAST [11, 12], T-10 [13], HL-2A [14], J-TEXT [15, 16], KTX [17], SUNIST [18, 19], KSTAR [20], W7-X [21], LHD [22], and H-1NF [23], etc. The electrostatic probes are also frequently employed to provide the plasma potential, electron density and temperature and many other physical parameter measurements in the scape-off layer or divertor region [24–38].

EAST is a medium size superconducting tokamak with major radius $R_0 \leqslant 1.9$ m, minor radius $a \leqslant 0.45$ m, toroidal magnetic field $B_T \leqslant 3.5$ T, and plasma current $I_p \leqslant 1$ MA. EAST has been equipped with various heating and current drive systems, i.e., the ion cyclotron resonance frequency (ICRF) heating system, the lower hybrid wave (LHW) system, the electron cyclotron resonance heating (ECRH) system, and the neutral beam injection (NBI) system [39]. Since April 2021, EAST has upgraded its graphite lower divertor to the tungsten lower divertor.

The magnetic probe system [11, 12] and electrostatic probe system [28, 38] have already been installed on the EAST, but there is still room for improvement. For example, the regular high frequency magnetic probes can only provide 2D measurements, i.e., poloidal and radial measurements, and cannot measure the toroidal magnetic fluctuations. They are arranged relatively far away from each other, the highest toroidal mode number (n) that can be resolved is only $n = \pm 8$, and the regular high-frequency magnetic probes can only resolve the magnetic fluctuation below 350 kHz. With these shortcomings, the regular high frequency magnetic probes on EAST have a limited ability to measure the fine structures of the electromagnetic fluctuations in the EAST plasmas. The fast reciprocating probe diagnostic on EAST has a very small measuring range of the edge electrostatic fluctuations in the poloidal and toroidal directions. At present, there is no fixed electrostatic probe array to monitor the plasmas crossing the limiter and antennas of the auxiliary heating systems to the first wall of EAST. Developing the electrostatic probe array near the first wall region might be important for analyzing the impact of the plasma disruptions and large edge localized mode (ELM) outbreaks.

In order to complement the existing magnetic and electrostatic probes on EAST, we have recently developed a novel electromagnetic probe array (EMPA) diagnostic on EAST. The probe head of the EMPA diagnostic is at the front end of the EAST horizontal port P and near the first wall. The EMPA consists of 24 newly designed 3D magnetic probes and 20 electrostatic probes. Compared with the 2D measurement ability of the regular magnetic probes on EAST, the EMPA can provide additional toroidal magnetic fluctuation measurements. Due to the compact arrangement of the EMPA magnetic probes, it can resolve the toroidal mode number up to $n = \pm 112$, and, with careful design and a higher sampling rate of 2 MHz, the EMPA magnetic probes aim to measure higher frequency magnetic fluctuations. Furthermore, the plasmas crossing the limiter to the first wall can be measured after developing the EMPA electrostatic probes. Compared with the EMPA diagnostic, there is another kind of electromagnetic probe diagnostic which is much smaller, more common and usually mounted on the moving manipulator to measure the plasma filaments and other information in the SOL region [40–48]. Unlike this kind of electromagnetic probe, the EMPA with a much larger size is fixed near the first wall and behind the limiter.

In this work, we describe the newly developed EMPA diagnostic in EAST and its preliminary applications in the experiments. The remainder of this paper is organized as follows. Section 2 describes the mechanical system, electrical system, acquisition and control system, and the effective area calibration of the EMPA. In section 3, the preliminary applications with the EMPA in the EAST L-mode and H-mode discharges are shown. Finally, the summaries and future works are presented in section 4.

2. Diagnostic setup

The EMPA probe head consists of a magnetic probe array composed of 24 identical 3D magnetic probes and an electrostatic probe array composed of 20 electrostatic probes. To give an overall impression of the EMPA diagnostic system, a schematic is used to show how this diagnostic works, as shown in figure 1. The original electromagnetic signals are firstly measured by the EMPA probe head located in the vacuum vessel; and then they are transmitted to the diagnostic signal extraction unit through the signal lines; and finally, they arrive at the data acquisition unit where they will be uploaded to the data server. The diagnostic control unit can flexibly control the working state of the diagnostic. Next, the main subsystems of the EMPA diagnostic and the calibration of the effective area of the EMPA magnetic probes will be introduced in this section.

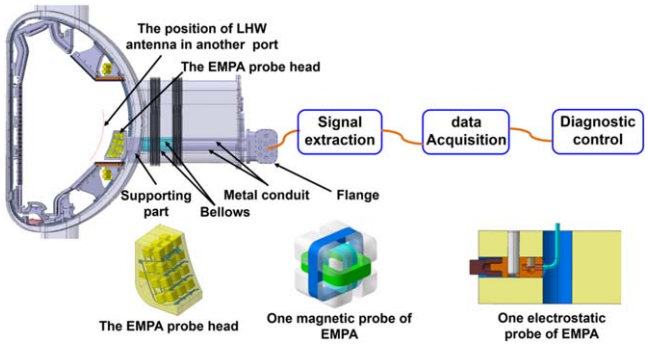

Figure 1. Schematic of the EMPA diagnostic system. A magnetic probe model and an electrostatic probe model of the EMPA probe head are shown in detail.

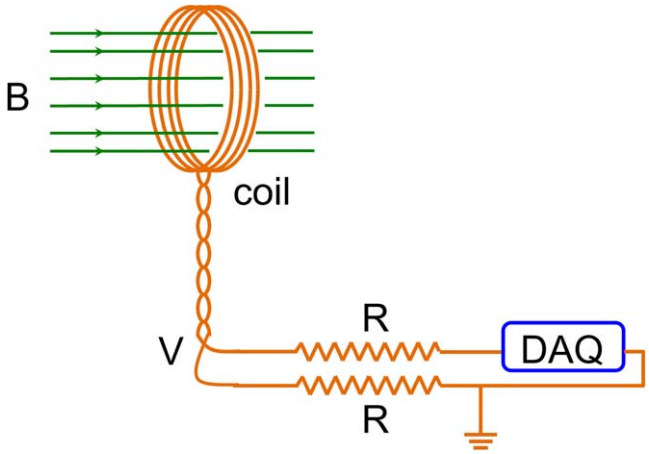

Figure 2. Schematic of a magnetic probe system.

Figure 3. Photo of an EMPA magnetic probe.

2.1. Mechanical system of the EMPA

The primary mechanical components of the EMPA inside the EAST vacuum vessel including magnetic probe array, electrostatic probe array and auxiliary supporting components are introduced here. In order to meet the challenges of the high vacuum, strong magnetic field, high heat and particle flux onto the wall in EAST, and to improve the signal-noise-ratio (SNR) of the EMPA diagnostic as much as possible, we have created many special designs and also safety analysis for the mechanical components of the EMPA diagnostic.

As shown in figure 2 and equation (1), when placing a small coil of wire into a changing magnetic field $B(t)$, an induced electromotive force $\varepsilon(t)$ in the wire will be generated. One can obtain the magnetic information by measuring the induced electromotive force, which is how the magnetic coil or named magnetic probe generally works [49, 50]. In equation (1), N is the number of turns in the coil area S.

$$\varepsilon(t) = -NS\frac{\mathrm{d}B(t)}{\mathrm{d}t} \tag{1}$$

One key measurement unit of the EMPA is the carefully designed 3D magnetic probe, which can measure the magnetic fluctuations in poloidal, radial and toroidal directions simultaneously, as illustrated in figures 1 and 3. Based on the size of the diagnostic window available for the EMPA and the bobbin space occupied by magnetic probe winding, we finally design the outer shape of the bobbin to be a cube with a side length of 45 mm. Each bobbin is made from high-temperature-resistant 95 alumina ceramics. The wire used for winding the magnetic probe is a customized enameled wire with a diameter of 1.2 mm, which is resistant to the high temperature, has low exhaust and is suitable for a vacuum environment. In the innermost region of the ceramic bobbin, four-layer windings with eight turns in each layer are applied to measure the magnetic fluctuations in the toroidal direction. In the middle region of the ceramic bobbin, four-layer windings with seven turns in each layer are applied to measure the poloidal magnetic fluctuations. In the outermost region of the ceramic bobbin, four-layer windings with six turns in each layer are applied to measure the magnetic fluctuations in the radial direction. Since higher effective area (NS) value usually increases the output amplitude of magnetic signals but lowers the cut-off frequency of the high frequency signal, the final design of the diameter of the enameled wire and the number of coil turns and layers for each magnetic direction, as mentioned above, is a compromise between the output amplitude and cut-off frequency of the high frequency signal.

The magnetic probe array of the EMPA consists of 24 identical 3D magnetic probes as mentioned above, and their spatial arrangement is shown in figure 4. The magnetic probe array is divided into two parallel layers of magnetic probes with a radial distance of 63 mm. The arc surfaces formed by each layer of magnetic probes are approximately parallel to the last closed magnetic flux surface of a typical H-mode discharge, and each layer of magnetic probes is placed in four poloidal rows and three toroidal columns, with a closest poloidal distance of ~ 78 mm between two magnetic probes and a closest toroidal distance of ~ 70 mm. The two-layer magnetic probe design of the EMPA is dedicated to measuring the radial gradient of magnetic fluctuations, analyzing the

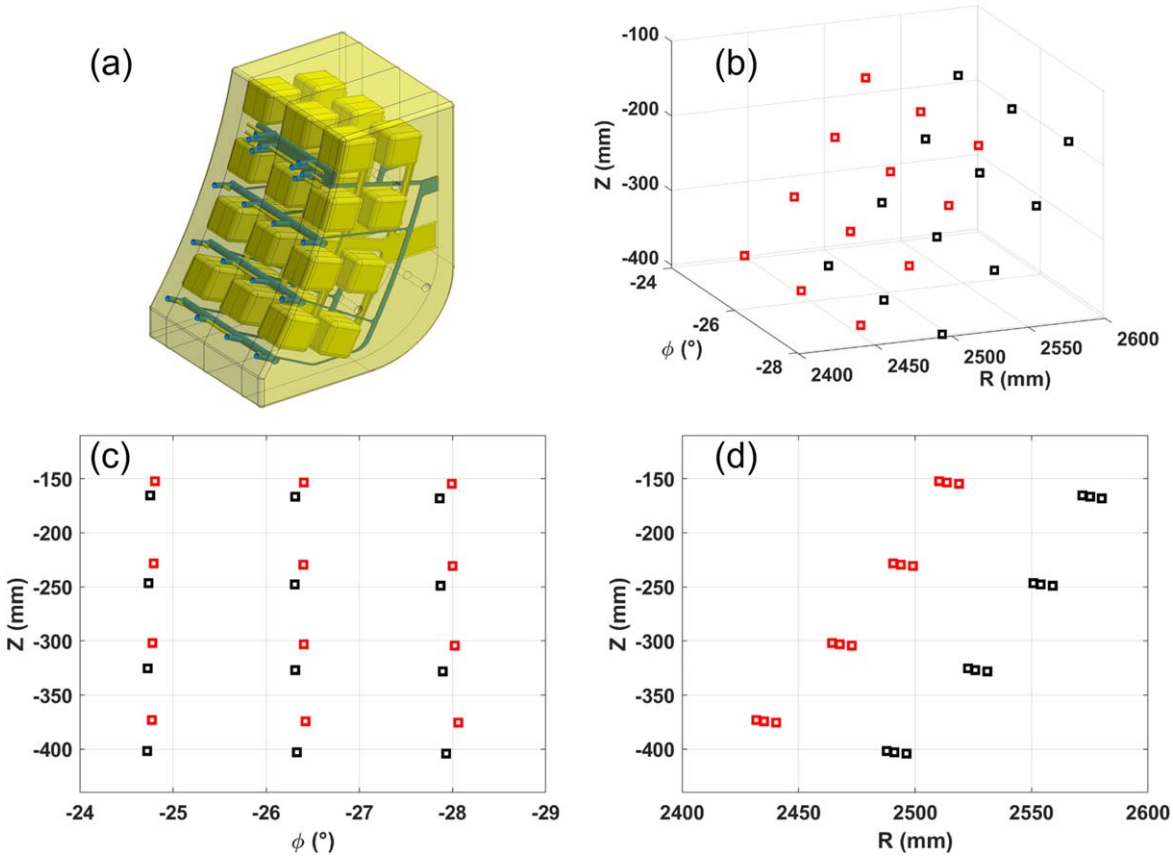

Figure 4. (a) Model of the EMPA magnetic probes, (b)–(d) positions of the EMPA magnetic probes in different coordinates with red and black squares representing the first and second layers of the magnetic probes, respectively.

attenuation of magnetic fluctuations along the radial direction, and attempting to infer the perturbed plasma current [44, 51–53]. The compact arrangement of the magnetic probe array in the poloidal and toroidal directions facilitates the high toroidal mode number and high poloidal wave number measurements of the magnetic fluctuations. The minimum toroidal angular distance between the magnetic probes is approximately 1.6°, and in theory, the magnetic probe array could detect the highest toroidal mode number $n = \pm 112$.

The electrostatic probe array of the EMPA consists of 20 identical graphite probes, each with a diameter of 5 mm, and protruding about 4 mm from the ceramic surface, as shown in figure 1. The electrostatic probe array is divided into two sets of four-tip probes and a single-tip probe array arranged in three poloidal rows and four toroidal columns, as shown in figure 5. Each four-tip probe consists of two floating potential probes placed 18.8 mm apart along the poloidal direction, and a dual probe placed 0.466° apart along the toroidal direction. As to the single-tip electrostatic probe array, the closest distance between two electrostatic probes in the poloidal direction is about 65.5–68.5 mm, and 1.27°–1.32° in the toroidal direction. The probes in the single-tip probe array are independent of each other, which can provide the floating potential or ion saturation current measurements.

The auxiliary supporting components of the EMPA used in the vacuum vessel are mainly 95 alumina ceramics and 316L nonmagnetic stainless steel. The 95 alumina ceramics are a nonconducting material which can withstand high particle and heat fluxes from the plasmas; and the 316L stainless steel is a nonmagnetic material which can avoid magnetization by EAST strong magnetic field. As shown in figures 1 and 5(a), all the EMPA magnetic probes and electrostatic probes are located inside the four customized 95 alumina ceramic blocks, which contain specially designed wire channels for signal transmission. In order to minimize the interference of the conductive materials on the magnetic probes, we only use three bolts to fix the four ceramic blocks; and a 316L stainless steel plate of 5 mm thickness, deliberately designed with many hollow structures, is used to support each of the whole ceramic blocks. Two 316L stainless steel tubes with different radii are connected at the back end of the EMPA probe head. The signal wires of the EMPA magnetic probe array are placed in the large stainless steel tube, while the signal wires of the EMPA electrostatic probe array are placed in the small stainless steel tube, which might reduce the possible interference of the electrostatic probe signals on the magnetic probe signals.

Before finally determining the installation position of the EMPA in the vacuum vessel, we also did the safety analysis of the effects of the EMPA on EAST experimental operations and the safety analysis of the EMPA itself. Based on the physical and engineering design parameters of the EMPA, it can be concluded that the EMPA has little impact on the safe

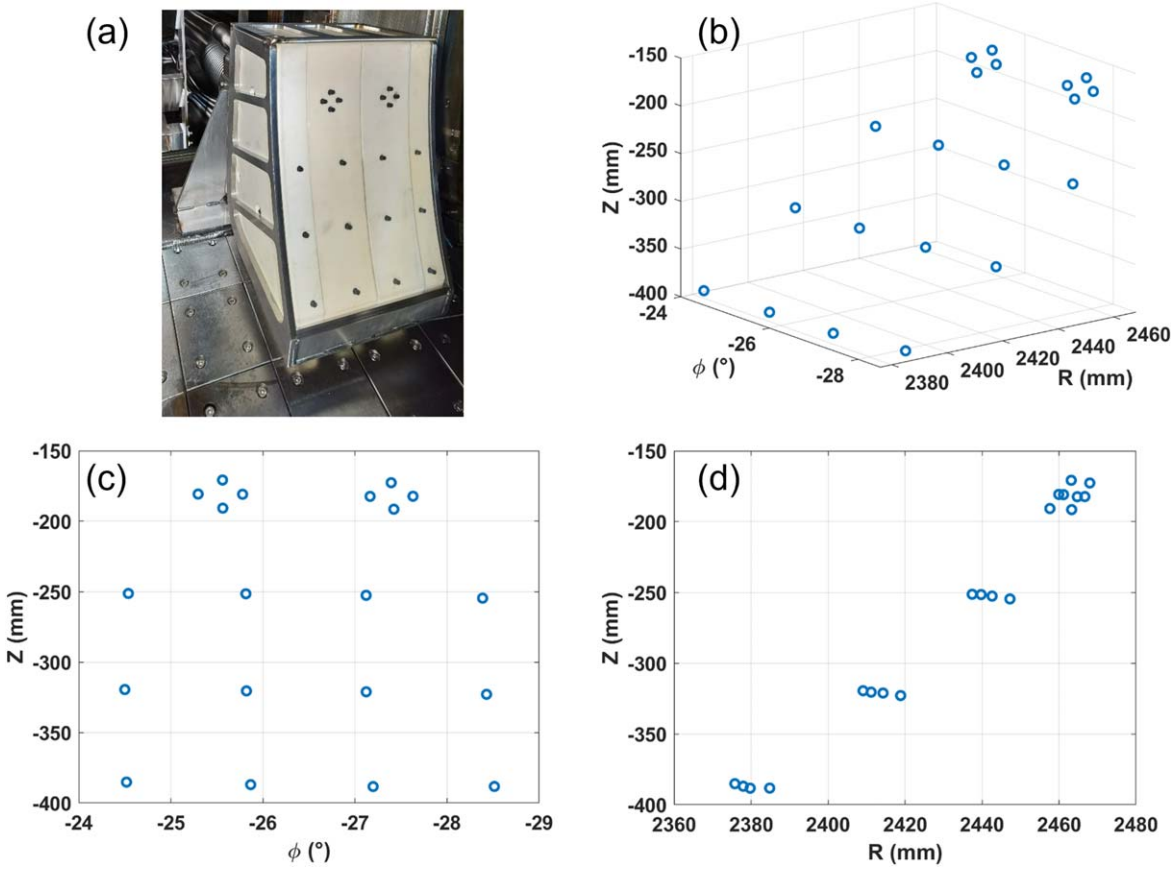

Figure 5. (a) Photo of the EMPA probe head showing its electrostatic graphite probes, (b)–(d) positions of the EMPA electrostatic probes in different coordinates.

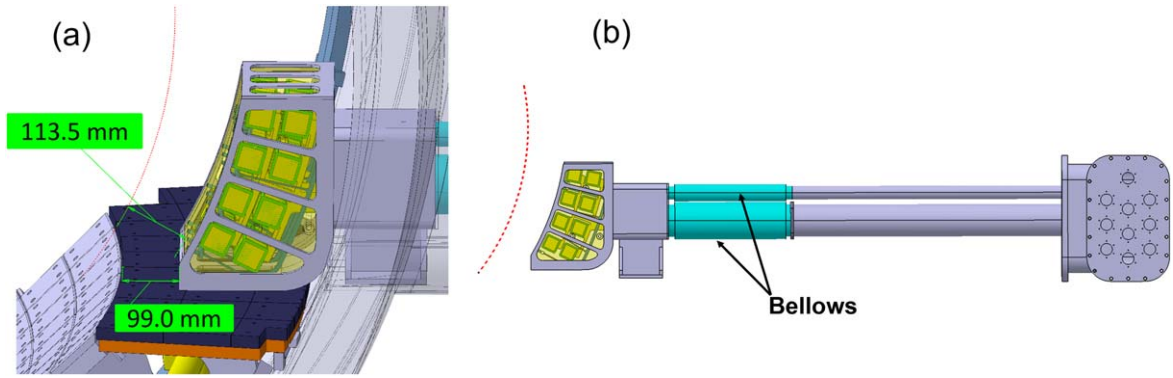

Figure 6. Some detailed designs of the EMPA for safe operation.

operation of EAST for the following reasons. (1) As shown in figure 6(a), the front end of the EMPA probe head is 99.0 mm behind the front end of the horizontal passive plate; and from the poloidal cross-sectional view, the closest distance between the front end of the EMPA probe head and the LHW antennas, located at EAST horizontal ports B and E, respectively, as indicated by the red dashed line, is 113.5 mm; these distances are large enough for EAST operation. (2) In normal discharges, the number of runaway electrons quickly decreases after the limiter; and in the disruptive discharges, it is possible that some runaway electrons may cross the limiter to the EMPA probe head. But in general, runaway electrons have little influence on the current designed EMPA probe head and this in turn indicates that the very limited damage to the EMPA probe head caused by the runaway electrons has little influence on the operation of EAST [54]. (3) Simulation analysis shows that fast ions deposit near the limiters of each auxiliary wave heating antenna, and the number of fast ions decreases quickly after crossing the limiters [55], which has little influence on the current designed EMPA probe head.

The current designed EMPA probe head itself is secured for the following reasons. (1) The main part of the EMPA probe head is made of alumina ceramics, which is wrapped with a 5 mm stainless steel plate. Thus, the ceramics will not easily fall off even if they are broken. (2) The front supporting components of the EMPA probe head are fixed on the front end of the horizontal port. The two stainless steel tubes of the EMPA probe head are fixed on the flange, which is located on the end of the horizontal port. In order to accommodate the relative shift between the EMPA probe head and the two stainless steel tubes due to the small displacement of the vacuum vessel during the plasma discharges, two 316L stainless steel bellows are used to connect the EMPA probe head and the two stainless steel tubes, as shown in figure 6(b).

The EMPA diagnostic has been working for three EAST experimental campaigns since 2021, and the designs are proved to be safe in practice.

2.2. Electrical system of the EMPA

This section mainly describes the signal line connections of the EMPA diagnostic, as shown in figure 7. As for the magnetic probe array of the EMPA, we deliberately keep the wires long enough for the magnetic coil winding, so we can twist the remaining wires and connect them to the vacuum feedthroughs on the flange, which is located at the end of the horizontal port. The EMPA has 24 identical 3D magnetic probes. The lengths of the wire to wind the EMPA magnetic probe in the poloidal, radial and toroidal directions are all different. But for all the EMPA magnetic probes in each direction, the same length of wire is used. This is good for analyzing the phase differences between the magnetic probes with the same measuring direction but located at different positions, and reducing the nonphysical errors. After the magnetic probe signals passing through the vacuum feedthroughs, the 6.6 m customized shielded twisted-pair cables are used to transmit signals. In order to facilitate the connection to the signal acquisition unit, the end of the twisted-pair cables is connected with short shielded coaxial cables, whose connectors can be easily connected to the data acquisition unit.

As for the electrostatic probe array of the EMPA, the same length of enameled wires is used to connect the probe tips to the vacuum feedthroughs. After the electrostatic probe signals passing through the vacuum feedthroughs, the 7 m customized shielded coaxial cables are used to transmit the signals to the signal extraction unit, where the electrostatic signals are extracted either through the circuit of the four-tip probe or the circuit of the single-tip probe. Finally, the extracted signals travel through the opto-isolators and reach the data acquisition unit.

For the signal line connections of the EMPA diagnostic, we carefully avoided looping the signal wires, in order to avoid coupling unwanted interference signals. We have gathered all the shielding ground wires of the EMPA magnetic and electrostatic probes to a single point, and then connected it to the dedicated diagnostic ground of EAST, which

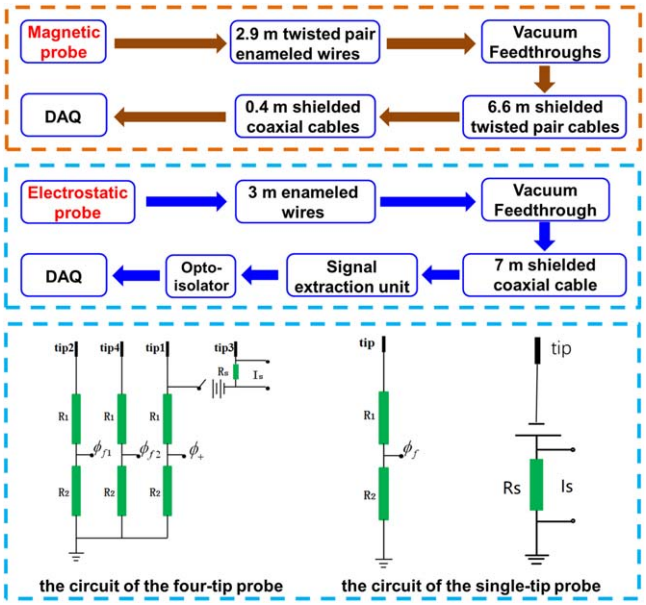

Figure 7. Schematic of the signal line connections of the EMPA diagnostic.

can largely reduce the interference from other systems around the EMPA diagnostic.

2.3. Acquisition and control systems of the EMPA

The acquisition and control systems of the EMPA are customized, which enable large data acquisition and storage at thousand-second timescale plasma discharges.

The data acquisition system of the EMPA uses the PXIe-1705 chassis and PXIe-8135 controller from National Instruments Corporation (NI corporation), and it has six data acquisition cards in total, including five PXIe-6358 data acquisition cards from NI corporation, whose sampling rate is 1.25 MS/s; and one 2 MS/s data acquisition card from Shanghai Jianyi Technology Co., Ltd with model number JY2005312-01. Each data acquisition card can acquire 16 channel signals simultaneously, and the EMPA has 92 channel signals in total. In order to meet the multi-channel and high-sampling rate data acquisition requirements of the EMPA, we also specially configured a high-speed memory card with a model number of PXIe-8304-2T, reading speed of 6.0 GB/s, writing speed of 6.0 GB/s, and capacity of 2 T.

There are two controlling modes for the data acquisition system of the EMPA, i.e., the remote mode and local mode. In the remote mode, EMPA automatically acquires data after receiving the trigger signal from the EAST operation control. If the acquisition time is less than the default value (such as 34 s), the acquired data will be uploaded to the EAST experimental data server automatically, or the acquired data will be stored in the local computer. The data sampling rate and acquisition trigger time can be modified based on the experimental requirements. In the local mode, one needs to manually set the discharge number and trigger the EMPA to start acquiring data, and the acquired data will

Table 1. Calibrated effective areas (*NS*) of all the EMPA 3D magnetic probes.

Serial number of the EMPA magnetic probe	*NS* value in toroidal direction (m^2)	*NS* value in poloidal direction (m^2)	*NS* value in radial direction (m^2)
1	0.02764	0.03284	0.03913
2	0.02741	0.03279	0.03892
3	0.02759	0.03290	0.03881
4	0.02755	0.03337	0.03889
5	0.02801	0.03378	0.03955
6	0.02842	0.03373	0.03924
7	0.02706	0.03244	0.03829
8	0.02763	0.03274	0.03864
9	0.02789	0.03288	0.03859
10	0.02769	0.03352	0.03949
11	0.02807	0.03403	0.03945
12	0.02827	0.03351	0.03942
13	0.02832	0.03353	0.03902
14	0.02851	0.03356	0.03954
15	0.02812	0.03259	0.03845
16	0.02808	0.03353	0.03988
17	0.02708	0.03305	0.03875
18	0.02841	0.03334	0.03946
19	0.02734	0.03267	0.03832
20	0.02811	0.03354	0.03942
21	0.02777	0.03391	0.03819
22	0.02706	0.03215	0.03812
23	0.02619	0.03277	0.03793
24	0.02748	0.03248	0.03772

be stored in the local computer. This mode is very convenient for debugging the EMPA diagnostic, e.g., to find the reasons why the EMPA signal is sometimes noisy during the experiment.

We also put another computer at the corner of the EAST experimental hall, where the interference from other systems is relatively low. The role of this computer is to control the power distribution unit (PDU) which provides power access for the EMPA data acquisition system. Thus, we can remotely restart the EMPA data acquisition system by remotely controlling the PDU through this dedicated computer. This helps a lot during the EAST experimental periods when the EMPA data acquisition system needs a restart.

2.4. Effective area calibration of the EMPA

The effective areas (*NS*) of all the 3D magnetic probes of the EMPA diagnostic have been calibrated with a long solenoid and a standard magnetic probe [50], as shown in figure 8. The solenoid is 1 m long with an inner diameter of 20 cm. A 200 Hz AC power supply is applied to the solenoid to generate a changing magnetic field. As shown in figure 2 and equation (1), when putting a magnetic probe into a changing magnetic field created by the energized solenoid, an induced electromotive force will be generated in the magnetic probe. During the *NS* calibration of the EMPA magnetic probes, a standard magnetic probe with known effective area N_0S_0 and

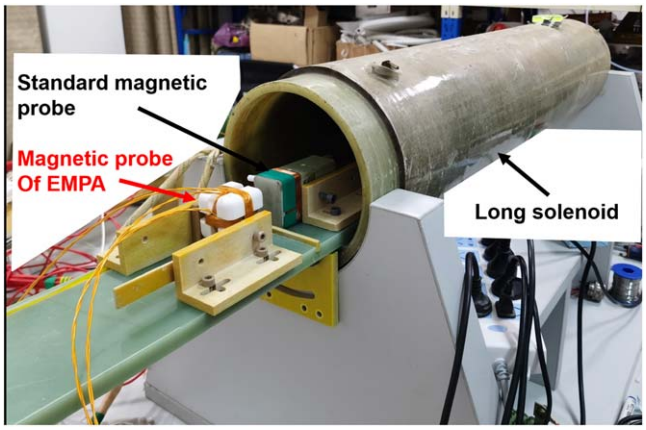

Figure 8. Energized long solenoid and standard magnetic probe used for the effective area (*NS*) calibration of the EMPA magnetic probes.

the EMPA magnetic probe, to be measured as an effective area *NS,* are placed in the center of the energized solenoid. A data acquisition system is used to acquire the time evolution information of the induced electromotive forces (ε_0, ε) of the standard magnetic probe and EMPA magnetic probe, respectively. Finally, the *NS* value of the EMPA magnetic probe can be obtained by comparing the ratio of the induced electromotive forces between the standard magnetic probe and the EMPA magnetic probe in the frequency domain. The detailed calibrated *NS* values of the EMPA magnetic probes are shown in table 1, which are consistent with our previous design, and are about half that of the EAST regular high frequency magnetic probe.

3. Preliminary experimental results

The EMPA diagnostic has been successfully applied to the 2021–2022 EAST experimental campaigns. Preliminary analysis of the EMPA data shows that it works well and can contribute to the experimental magnetic and electrostatic fluctuations studies.

Firstly, we take a common L-mode discharge #98276 on EAST, as an example, to analyze and discuss the EMPA data. This discharge has a double null divertor configuration with $B_{T0} \approx -2.46$ T. As shown in figure 9, this discharge has a plasma current of 0.5 MA and line average density of 0.2×10^{20} m^{-3}. It is heated by two LHW heating systems in the frequency of 2.45 GHz and 4.6 GHz with source powers of 0.8 MW and 2.0 MW respectively. The plasma stored energy of this discharge is about 97 kJ, and the divertor D_α radiation is used to monitor the edge particle recycling characteristics. Figure 9(e) shows the time evolution of the floating potential measured by the EMPA electrostatic probe, and the time evolution of the poloidal magnetic fluctuation measured by the EMPA magnetic probe is shown in figure 9(f). The raw data of the poloidal magnetic fluctuation and its spectrogram measured by the EAST regular high frequency magnetic probe are shown in figures 9(g) and (h) respectively. As shown in figures 9(f) and (g), the raw data

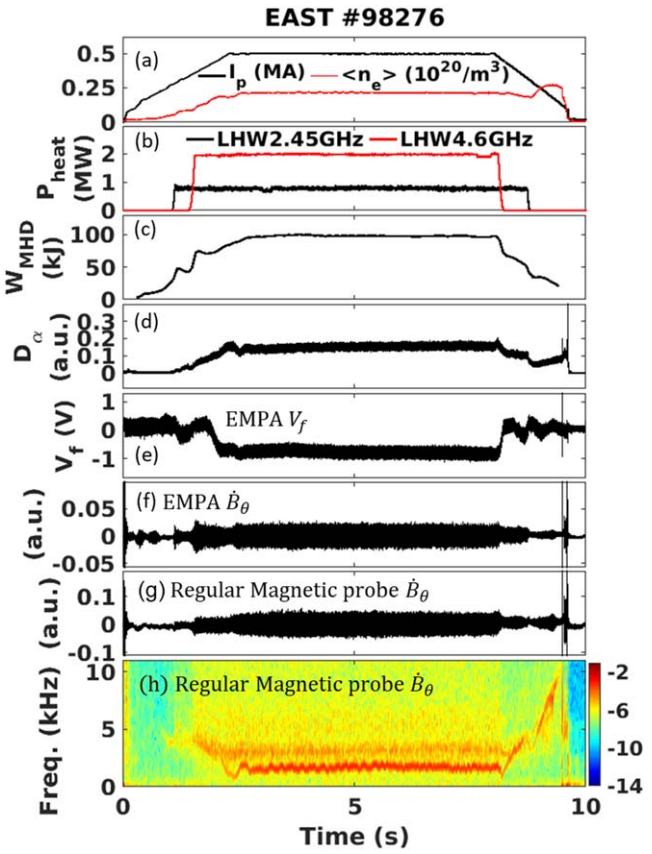

Figure 9. Time evolution of the (a) plasma current (black), line averaged density (red), (b) source power of the LHW heating, (c) plasma stored energy, (d) divertor D_α signal, (e) EMPA measured floating potential, (f) EMPA measured poloidal magnetic signal, (g) EAST regular magnetic probe signal and (h) its spectrogram of the discharge #98276.

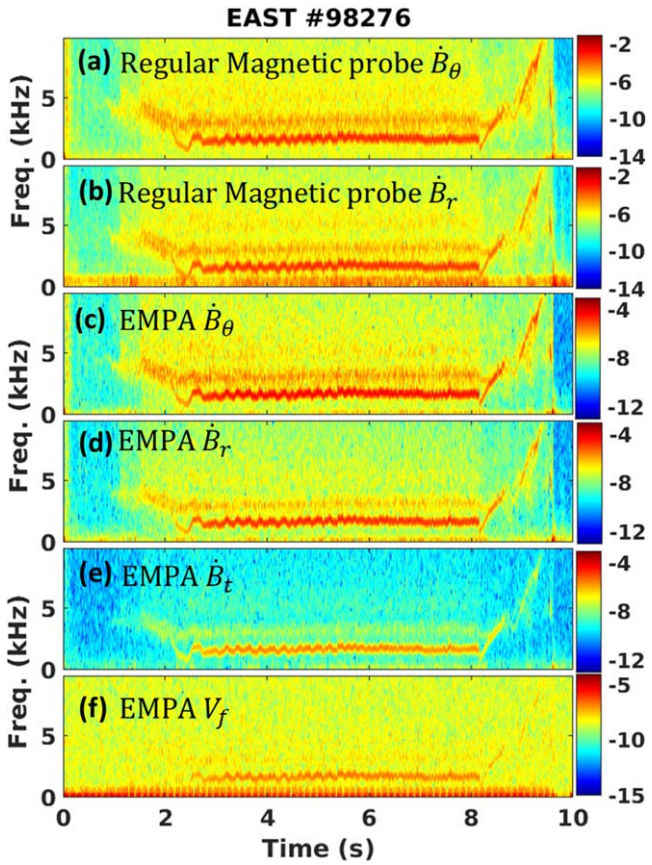

Figure 10. Spectrograms of the signals measured by the EAST regular magnetic probe, EMPA magnetic probe and EMPA floating potential probe.

measured by the EMPA magnetic probe are very similar to the raw data measured by the EAST regular magnetic probe indicating that the EMPA magnetic probe works properly. From figure 9(h), we can see that there are two MHD fluctuations with frequencies of 2.0 kHz and 3.2 kHz during this discharge.

In addition, the spectrograms of the signals measured by the EAST regular magnetic probe in all directions, EMPA magnetic probe and EMPA floating potential probe are shown in figure 10. We can see that the MHD fluctuations in the frequencies of 1.7 kHz and 3.0 kHz are observed by all the magnetic probes and in all directions, i.e., in poloidal, radial, and toroidal directions. It can be noted that the EMPA magnetic probe can provide additional toroidal magnetic fluctuation measurement capability compared with the regular magnetic probe on EAST, as shown in figure 10(e). Due to the strong amplitude of the magnetic fluctuation in the frequency of 1.7 kHz, it is also measured by the EMPA floating potential probe near the first wall of EAST, as shown in figure 10(f).

The toroidal mode numbers of the MHD fluctuations are calculated with two EMPA magnetic probes located at $Z \approx -374$ mm, $R \approx 2436$ mm and toroidally separated by 3.286° as shown in figure 11(a). The MHD fluctuation in the frequency of 1.7 kHz has a toroidal mode number $n = -2$, while the MHD fluctuation in the frequency of 3.0 kHz has a toroidal mode number $n = -1$, where the minus sign represents the countercurrent propagation direction. As shown in figure 11(c), the toroidal mode numbers of the MHD fluctuations measured by the EAST regular magnetic probes are very similar to the EMPA measurements indicating that the EMPA magnetic probes work well and can be used for the toroidal mode number analysis.

One feature of the EMPA is that the EMPA magnetic probe array can be applied to the propagation studies of the magnetic fluctuations in 2D or even 3D directions. Here, we take the $n = -2$ MHD mode, as mentioned in figure 11, as an example for the following analysis. Figure 12 shows the poloidal and toroidal propagations of the radial magnetic fluctuation measured by the first layer of the EMPA magnetic probes, whose positions are depicted by red squares in figure 4. The data shown in figure 12 are taken from the discharge #98276 in $t = 5.969$–5.972 s and filtered in the frequency band of 1.4–2 kHz, similar to the frequency range of $n = -2$ MHD mode. As indicated by the red arrows in figure 12, in each toroidal direction, i.e., $\phi = -28.1°$, $\phi = -26.4°$, and $\phi = -24.8°$, the $n = -2$ MHD mode propagates poloidally from $Z = -154$ mm to $Z = -374$ mm.

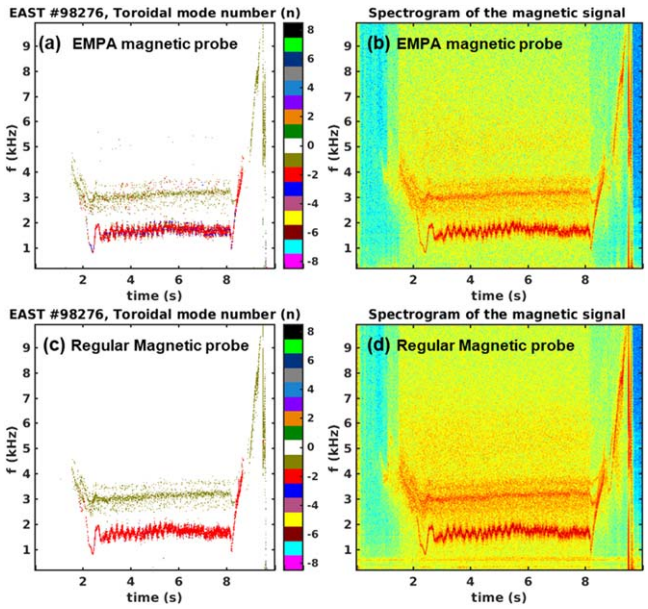

Figure 11. (a) and (b) Toroidal mode number and spectrogram of the magnetic fluctuations measured by the EMPA magnetic probes, (c) and (d) toroidal mode number and spectrogram of the magnetic fluctuations measured by the EAST regular magnetic probes.

Next, we take an example to show that the EMPA can also contribute to the H-mode studies on EAST. As shown in figure 13, this is an H-mode discharge with plasma current $I_p = 0.5$ MA, line average density of $(3.4 - 4.2) \times 10^{19}$ m^{-3}. The plasma stored energy increased slightly after $t = 7.1$ s, and the bursting amplitude of the divertor D_α radiation which is used to monitor the ELM behavior was increased. As shown in figure 13(e), the bursting amplitude of the floating potential measured by the EMPA electrostatic probe near the first wall was also clearly increased. From the spectrograms of the signals measured by the EMPA magnetic probe and EAST regular high frequency magnetic probe as shown in figures 13(l) and (m), clear high frequency broadband (200–600 kHz) magnetic fluctuations were observed during the inter-ELM periods, and they were terminated by the ELM bursts. The inter-ELM magnetic fluctuations might be correlated with the pedestal evolution during the inter-ELM period [56, 57], but the nature of the high frequency (200–600 kHz) magnetic fluctuations is still unclear in EAST. More detailed studies on the magnetic fluctuations with the newly developed EMPA will be conducted in our future work. Besides the higher sampling rate of the EMPA magnetic probe, the resonance frequency of the EMPA magnetic probe as indicated by the blue arrow seems to be higher than the resonance frequency of the EAST regular high frequency magnetic probe, as shown in figures 13(g) and (h). The magnetic fluctuations with high mode numbers tend to have higher signal frequencies. With higher frequency resolution and toroidal mode measurement capability, the EMPA can be used to study higher frequency magnetic fluctuations in the future. We also note that the floating potential measured by the EMPA near the first wall can reflect the large ELM bursts as shown in figures 13(i) and (j), which might contribute to the studies of the effects of ELMs on the first wall. Thus, we plot the figures 14(a)–(k) to show the time evolution of the floating potentials in different poloidal and toroidal locations measured by the EMPA single-tip probe array near the first wall in this discharge. Figure 14(l) is the D_α trace at the same time period as the floating potentials. As shown in figure 14, the effects of the ELMs on the area monitored by the EMPA floating potential array in this discharge do not show clear differences in poloidal or toroidal directions. More works are still needed to study this topic.

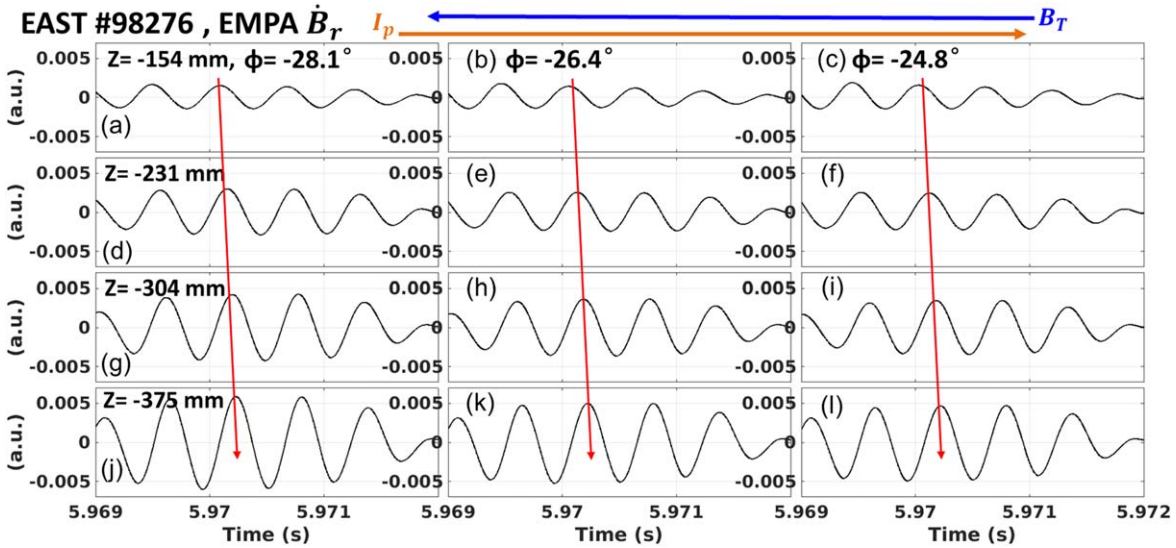

Figure 12. Time evolutions of the radial magnetic fluctuations in different poloidal and toroidal locations, measured by the first layer of EMPA magnetic probes. The data shown here are taken from the discharge #98276 in $t = 5.969$–5.972 s and filtered in the frequency band of 1.4–2 kHz. The orange and blue arrows show the toroidal propagation directions of I_p and B_T respectively.

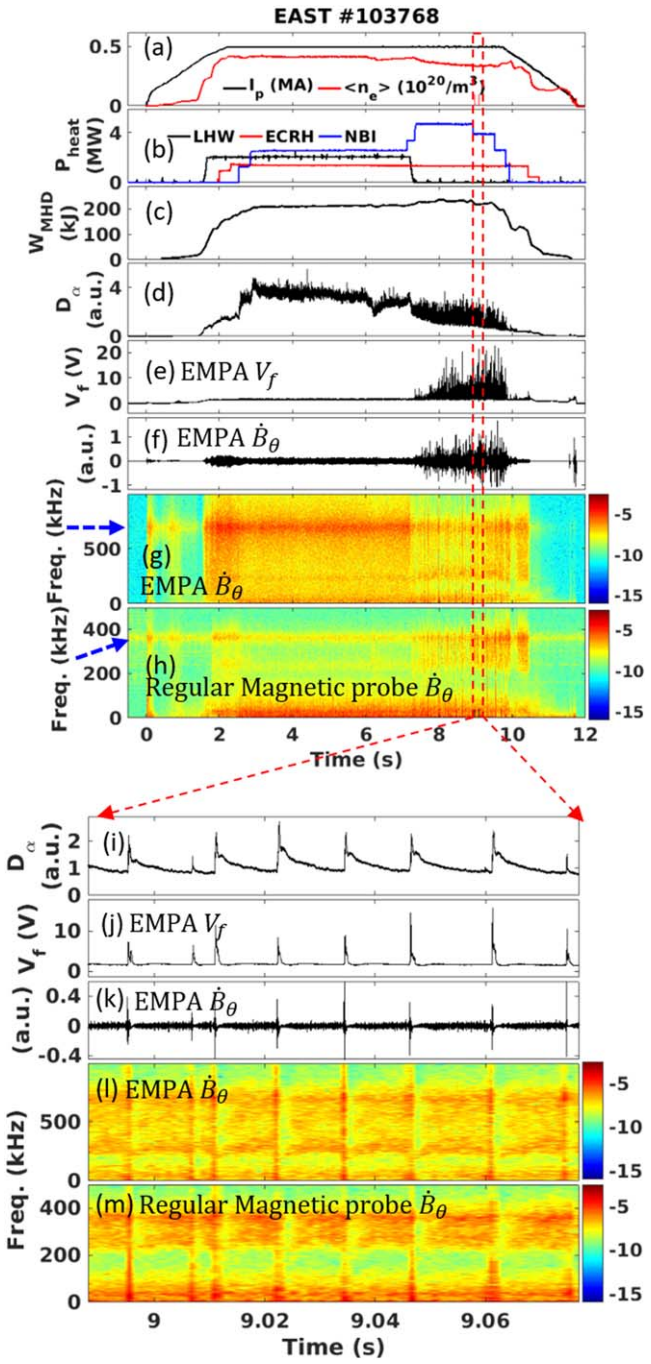

Figure 13. Time evolutions of the (a) plasma current (black), line averaged density (red), (b) source power of different heatings, (c) plasma stored energy, (d) divertor D_α signal, (e) EMPA measured floating potential, (f) EMPA measured poloidal magnetic signal and (g) its spectrogram and (h) spectrogram of EAST regular magnetic probe signal in the discharge #103768. (i)–(m) Zoom-in plots of the signals in (d)–(h).

4. Summary and outlook

A novel electromagnetic probe array (EMPA) diagnostic has been successfully developed on EAST. The specially designed mechanical system, electrical system, acquisition and control system, and the *NS* calibration of the EMPA are introduced in this paper. The EMPA is fixed near the first wall at horizontal port P. The EMPA consists of two parallel layers of magnetic probes with a radial distance of 63 mm and one electrostatic probe array with 20 electrostatic probes. Each layer of magnetic probes consists of 12 identical magnetic probes arranged in four poloidal rows and three toroidal columns. Every single magnetic probe can measure the magnetic fluctuations in three directions, i.e., the toroidal, poloidal, and radial directions, which provides the additional toroidal measurements compared with the regular magnetic probes on EAST. The highest sampling rate of the EMPA magnetic probes is 2 MHz, which improves the ability to measure high frequency magnetic fluctuations compared with the EAST regular high frequency magnetic probes, whose sampling rate is 1 MHz. The smallest poloidal distance between the magnetic probes of the EMPA is 78 mm, which is smaller than the distance between regular high frequency magnetic probes on EAST, and capable of measuring the high frequency magnetic fluctuations with higher poloidal wave numbers. The smallest toroidal angle difference between the magnetic probes of the EMPA is $\sim$1.6°, and in theory, it can measure the magnetic fluctuations with the toroidal mode number $-112 \leqslant n \leqslant 112$, which is far beyond the toroidal mode number measurement capability of EAST regular magnetic probes with $-8 \leqslant n \leqslant 8$. The electrostatic probe array of the EMPA consists of two sets of four-tip probes and one single-tip probe array which is arranged in three poloidal rows and four toroidal columns, and the electrostatic probe array of the EMPA can measure the electrostatic parameters, such as floating potential and ion saturated current etc, near the EAST first wall.

Preliminary application of the EMPA in the L-mode discharge on EAST shows that it works well for providing the spectrogram information of the electrostatic signal and 3D magnetic signals, and the toroidal mode numbers and poloidal propagation information of the magnetic fluctuations in the L-mode discharge can be provided by the EMPA. Preliminary application of the EMPA in the H-mode discharge on EAST shows that it works well for measuring the high frequency pedestal fluctuations and providing information on the ELM events near the EAST first wall.

In the near future, careful frequency response analysis of EMPA magnetic probes will be conducted, when the LCR digital bridge with a working frequency of up to 2 MHz is available. The scanning power supply will be applied to the electronic circuit of the EMPA electrostatic probe array to obtain its current-voltage characteristic, and more effort will be taken to study the EMPA electrostatic probe data and to derive the T_e and n_e information in the experiments. The ELM and disruption characteristics will be studied with EMPA-measured ion saturation currents and floating potentials in the future experiments [58, 59]. Deeper analysis of the EMPA data already measured in the EAST experiments will be conducted, e.g., deriving the fine structure of current filaments with the EMPA data, and studying the detailed characteristics of Alfvén eigenmodes and high frequency pedestal fluctuations in EAST plasmas.

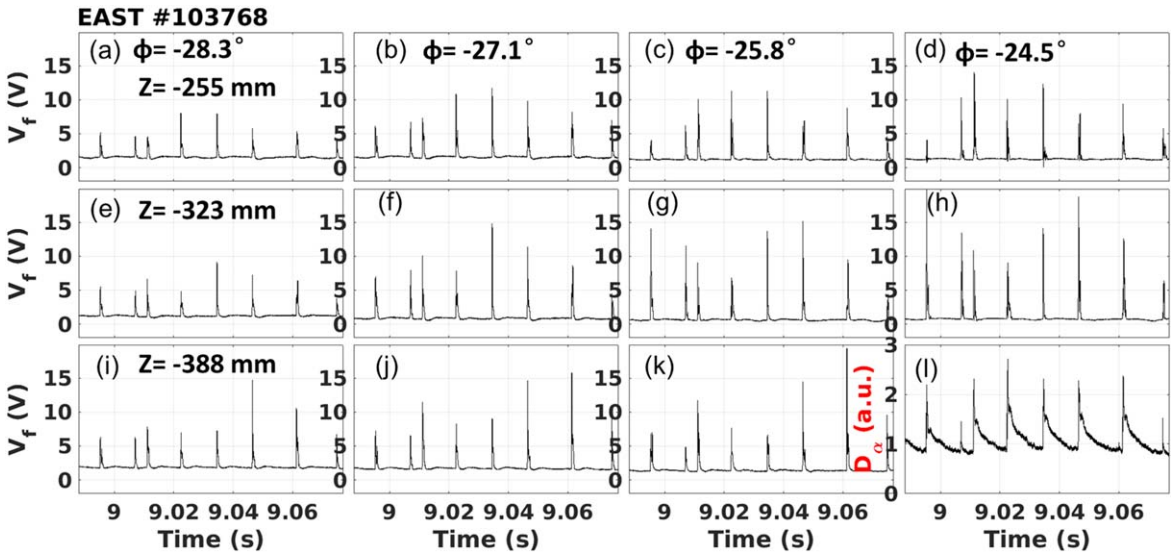

Figure 14. Time evolutions of the floating potential in different poloidal and toroidal locations measured by the EMPA single-tip probe array. The data shown here is taken from the discharge #103768 in t = 8.99–9.08 s and filtered by a low-pass filter with a cutoff frequency of 6 kHz.

Acknowledgments

One of the authors (Heng Lan) gratefully acknowledges valuable discussions and support from the EAST team, including Ruijie Zhou, Yingfeng Xu, Dalong Chen, Lixing Chen, Biao Shen, Kai Hu, Xigui Gu, Zhongming Lu, Qi Wang, Qingzhao Qu, Niu Jin, *et al.* This work is supported by the National Magnetic Confinement Fusion Energy R&D Program of China (Nos. 2019YFE03030000 and 2022YFE03020004), National Natural Science Foundation of China (Nos. 12105187, 11905250 and 11975275), the China Postdoctoral Science Foundation (No. 2021M702245), and the Users with Excellence Program of Hefei Science Center, CAS (No. 2021HSC-UE014).

ORCID iDs

Pengfei ZI (訾鹏飞) https://orcid.org/0000-0001-5393-135X

References

[1] Strait E J 2006 *Rev. Sci. Instrum.* **77** 023502
[2] King J D *et al* 2014 *Rev. Sci. Instrum.* **85** 083503
[3] Basse N P *et al* 2007 *Fusion Sci. Technol.* **51** 476
[4] Gerhardt S P *et al* 2014 *Rev. Sci. Instrum.* **85** 11E807
[5] Artaserse G *et al* 2019 *Fusion Eng. Des.* **146** 2781
[6] Gernhardt J 1992 Magnetic diagnostic on ASDEX upgrade with internal and external pick-up coils (IPP 1/262) Garching (DE): Max-Planck-Institut für Plasmaphysik
[7] Giannone L *et al* 2013 *Fusion Eng. Des.* **88** 3299
[8] Hole M J *et al* 2009 *Rev. Sci. Instrum.* **80** 123507
[9] Moret J M *et al* 1998 *Rev. Sci. Instrum.* **69** 2333
[10] Moreau P *et al* 2018 *Rev. Sci. Instrum.* **89** 10J109
[11] Shen B *et al* 2003 *Plasma Sci. Technol.* **5** 1785
[12] Liu G J *et al* 2013 *Rev. Sci. Instrum.* **84** 073502
[13] Savrukhin P V and Shestakov E A 2012 *Rev. Sci. Instrum.* **83** 013505
[14] Liang S Y *et al* 2017 *AIP Adv.* **7** 125004
[15] Li F M *et al* 2016 *Rev. Sci. Instrum.* **87** 11D436
[16] Han D L *et al* 2021 *Plasma Sci. Technol.* **23** 055104
[17] Tu C *et al* 2017 *Rev. Sci. Instrum.* **88** 093513
[18] Liu Y Q *et al* 2014 *Rev. Sci. Instrum.* **85** 11E802
[19] Cheng Z B *et al* 2021 *Rev. Sci. Instrum.* **92** 053518
[20] Lee S G *et al* 2008 *Rev. Sci. Instrum.* **79** 10F117
[21] Endler M *et al* 2015 *Fusion Eng. Des.* **100** 468
[22] Sakakibara S, Yamada H and LHD Experiment Group 2010 *Fusion Sci. Technol.* **58** 471
[23] Haskey S R *et al* 2013 *Rev. Sci. Instrum.* **84** 093501
[24] Wang W H *et al* 2005 *Plasma Phys. Control. Fusion* **47** 1
[25] Yan L W *et al* 2006 *Rev. Sci. Instrum.* **77** 113501
[26] Silva C *et al* 2009 *Plasma Phys. Control. Fusion* **51** 105001
[27] Tanaka H *et al* 2009 *Nucl. Fusion* **49** 065017
[28] Zhang W *et al* 2010 *Rev. Sci. Instrum.* **81** 113501
[29] Bak J G *et al* 2013 *Contrib. Plasma Phys.* **53** 69
[30] Fukumoto M *et al* 2013 *Plasma Fusion Res.* **8** 1405153
[31] LaBombard B *et al* 2014 *Phys. Plasmas* **21** 056108
[32] Killer C *et al* 2019 *Nucl. Fusion* **59** 086013
[33] Deng T J *et al* 2020 *Plasma Sci. Technol.* **22** 045602
[34] De Oliveira H *et al* 2021 *Rev. Sci. Instrum.* **92** 043547
[35] Watkins J G *et al* 2021 *Rev. Sci. Instrum.* **92** 053523
[36] Grenfell G *et al* 2022 *Rev. Sci. Instrum.* **93** 023507
[37] Huang Z H *et al* 2022 *Plasma Sci. Technol.* **24** 054002
[38] Meng L Y *et al* 2022 *Fusion Eng. Des.* **175** 113011
[39] Wan B N *et al* 2022 *Nucl. Fusion* **62** 042010
[40] Ionita C *et al* 2009 *J. Plasma Fusion Res. SERIES* **8** 413
[41] Spolaore M *et al* 2009 *J. Nucl. Mater.* **390-391** 448
[42] Chai S *et al* 2014 *Rev. Sci. Instrum.* **85** 11D804
[43] Yan N *et al* 2014 *Plasma Phys. Control. Fusion* **56** 095023
[44] Spolaore M *et al* 2015 *Phys. Plasmas* **22** 012310
[45] Drews P *et al* 2017 *Nucl. Fusion* **57** 126020
[46] Kovarik K *et al* 2017 *Rev. Sci. Instrum.* **88** 035106
[47] Agostinetti P *et al* 2018 *IEEE Trans. Plasma Sci.* **46** 1306
[48] Yang Q H *et al* 2022 *Plasma Sci. Technol.* **24** 054005
[49] Hutchinson I H 2002 *Principles of Plasma Diagnostics* 2nd edn (Cambridge: Cambridge University Press)

[50] Shen B and EAST Magnetic Diagnostics Team 2016 *Fusion Eng. Des.* **112** 969
[51] Spolaore M *et al* 2009 *Phys. Rev. Lett.* **102** 165001
[52] Furno I *et al* 2011 *Phys. Rev. Lett.* **106** 245001
[53] Vianello N *et al* 2011 *Phys. Rev. Lett.* **106** 125002
[54] Zhou R J *et al* 2017 *Nucl. Fusion* **57** 114002
[55] Xu Y F *et al* 2021 *Plasma Sci. Technol.* **23** 095102
[56] Lan H *et al* 2019 *Phys. Plasmas* **26** 122505
[57] Diallo A and Laggner F M 2021 *Plasma Phys. Control. Fusion* **63** 013001
[58] Dimitrova M *et al* 2016 *J. Phys. Conf. Ser.* **700** 012008
[59] Adamek J *et al* 2022 *Nucl. Fusion* **62** 086034